Nonlinear Dynamics and Systems Theory, **22** (1) (2022) 66–81

Similarities between the Lorenz Related Systems

C. Morel [1*], R. C. Vlad [2] and J.-Y. Morel [3]

[1] *Aeronautical and Automobile Engineering School, ESTACA'Lab Paris Saclay, France.*
[2] *Technical University of Cluj-Napoca, 103-105 Bd. Muncii, 400641 Cluj-Napoca, Romanie.*
[3] *University of Angers, 4 Bd. Lavoisier, 49100 Angers, France.*

Received: July 9, 2021; Revised: December 5, 2021

Abstract: In this paper, the dynamic behaviour of all the Lorenz related systems is examined in a previously unexplored region of parameter space. The Lorenz, hidden chaotic, Chen and broken butterfly attractors can be generated at any desired size, with different equilibria. We focus on the attractors smaller or larger than the original one, we call them *mini* and *maxi*, and study their global dynamic behaviour to demonstrate that they are similar or equivalent to the original chaotic attractor. We finally examine their phase portraits, bifurcation diagrams, the largest Lyapunov exponents and their multiscale entropy MSE_{1D}. The analysis results show that the mini, original and maxi Lorenz related attractors have the same MSE_{1D} values and are independent of the scale factor. We can conclude that the MSE_{1D} analysis can be used successfully to quantify the complexity of the dynamic response.

Keywords: *attractors; bifucation; equilibria; Lyapunov; entropy.*

Mathematics Subject Classification (2010): 37M22, 65P30, 70K42, 93D05, 94A17.

1 Introduction

Since the Lorenz system was discovered, chaos and many phenomena in nonlinear dynamic systems have been developed and studied. This allowed to explore more chaotic systems and to discover new chaotic systems with a more complex dynamic behaviour. Chen and Lü [1] found a similar but not equivalent chaotic attractor, the dual of the Lorenz system. After that, Lü [2] reported a new chaotic system which is the transition between the Lorenz and Chen systems. [3] presented a comparative analysis of the Lorenz and Chen systems in order to understand better what distinguishes them. It is

* Corresponding author: mailto:cristina.morel@estaca.fr

notable that for certain values of the parameters, the classical Lorenz butterfly attractor is broken into a symmetric pair of strange attractors [4].

Several complex dynamic systems, called multistable systems, are characterized by the existence of many coexisting attractors. In this kind of systems, the trajectory will eventually end in an attractor strongly influenced by the initial conditions. [5] introduced a new category of chaotic systems with a line of equilibria. The basin of attraction may intersect with the line of equilibria, in some sections. There are many examples of chaotic systems with no equilibrium [6], one stable equilibrium [7], a single unstable equilibrium [8], many equilibria, a line equilibrium [5], a surfaces of equilibria [9].

Most of the known chaotic attractors (like the Lorenz, Chua or Van der Pol ones) are located in the neighbourhood of unstable fixed points. Such attractors are called self-excited and their basins of attraction touch unstable equilibrium. The transient trajectory of the attractor starts in the neighbourhood of this unstable equilibrium, oscillates around and then traces it. The concept of hidden attractors has been suggested by the discovery of unexpected attractor in Chua's circuit. Recently, it has been shown that multistability is connected with the occurrence of hidden attractors. In multistable systems, particularly in the case of the existence of attractors with very small basins like in [9], the switching from one attractor to another unexpected attractor can be observed. Hidden attractors are important in engineering applications [10] because many physical structures can have disastrous responses to perturbations, as the crash of aircraft YF-22 Boeing in 1992. Other applications of chaos theory such as synchronization [11], [12] and chaos control of hyperchaotic financial model have become topics for research.

The Chen system, butterfly attractor broken into a symmetric pair and hidden attractor are named the Lorenz related systems because they are derived from the Lorenz system. We introduce a parameter γ in (2) describing these systems and study the influence of a variation of γ on the occurrence of such chaotic attractors and on their size. In this paper, we find that the chaotic attractors occurred are mini and maxi attractors. By changing the parameter γ, all the quantitative properties of the Chen, Lorenz, hidden and broken butterfly attractors are preserved. This is why, the Lorenz related systems are essentially the one-parameter systems.

The irregularity of time series can be studied through several measures, e.g., sample entropy ($SampEn_{1D}$), which improves the understanding of the nonlinear behaviour of complex systems. $SampEn_{1D}$ is the measure of the degree of irregularity and disorder of finite length time series; it evaluates the probability of finding similar patterns. $SampEn_{1D}$ is precisely the negative natural logarithm of the conditional probability that two sequences similar for m points remain similar at the next point, where self-matches are not included in the computation of the probability [13]. A lower value of $SampEn_{1D}$ indicates many similarities in time-series. However, $SampEn_{1D}$ is not adapted for structures at the multiple time scale. This is why the multiscale entropy MSE_{1D} has been proposed to extend the computation of $SampEn_{1D}$ over a range of time scales. The concept of multi-scale entropy is used to characterize the complexity of different research fields [14]. Serving as a quantification parameter, MSE_{1D} is based on the coarse-graining procedure that uses a coarse-grained time series, as an average of the original data points within not overlapping windows by increasing the scale factor τ.

In this paper, the dynamic behaviour of the Lorenz related systems is examined in a previously unexplored region of parameter space. By simulation, the attractors can be generated at different equilibria in the function of γ. Furthermore, the generated attractors (smaller than the original attractor called *mini* and bigger called *maxi*) are

similar to it but are not identical because of their chaotic behaviour. According to the Jacobian matrix of the nonlinear system, the local stability of the generated attractors is studied. In order to study the global dynamic behaviour, firstly, bifurcation diagrams and Lyapunov exponents are used to investigate the presence of chaos in the Chen system. The simulations reveal the same value of the largest Lyapunov exponent of the attractor's size. Secondly, multiscale entropy MSE_{1D} is proposed to evaluate the complexity of these mini, original and maxi chaotic attractors. MSE_{1D} is applied to different time series of the chaotic attractors to determine their irregularity over a range of temporal scales. The results show that the mini, original and maxi chaotic attractors have the same irregularity values for all time scales (i.e., the same complexity of the time series). More precisely, all the quantitative properties are preserved.

2 The Lorenz Related Systems

The Lorenz related systems are described by the following set of differential equations:

$$\begin{cases} \dot{x} = \sigma(y - x), \\ \dot{y} = \rho x - \alpha y - xz, \\ \dot{z} = xy - \beta z. \end{cases} \tag{1}$$

Lorenz found the first canonical chaotic attractor in a three-dimensional autonomous system. The usual values of the classical Lorenz system parameters are $\sigma = 10$, $\rho = 28$, $\alpha = 1$, $\beta = 8/3$; this produces a chaotic attractor with a butterfly shape. Then, a similar looking but nonequivalent chaotic attractor was found out, which is the dual of the Lorenz system. Moreover, both attractors occur for different values of the parameters ($\sigma = 35$, $\rho =$ -7, $\alpha =$ -28, $\beta = 3$). The work of Lü [2] introduced a unified chaotic system (Lü system) which bridges the gap between the Lorenz system and the Chen system. A hidden chaotic attractor was illustrated in the classical Lorenz system depending on the values of both system parameters and initial conditions ($\sigma = 4$, $\rho = 29$, $\alpha = 1$, $\beta = 2$). For some values of the parameters ($\sigma = 0.12$, $\rho = 0$, $\alpha = 1$, $\beta =$ -0.6), Li and Sprott [4] broke the classical butterfly attractor into a symmetric pair of strange attractors. In this paper, we introduce the parameter γ in (1)

$$\begin{cases} \dot{x} = \sigma(y - x), \\ \dot{y} = \rho x - \alpha y - \gamma xz, \\ \dot{z} = xy - \beta z. \end{cases} \tag{2}$$

Special sides of the system (2) are then pointed out: the attractor's size depends on the variation of the parameter γ in system (2). $\gamma \in$(0,1) leads to a chaotic attractor (called maxi) with a larger size than the original chaotic attractor of system (1) (i.e., for $\gamma =$ 1). Similarly, $\gamma > 1$ leads to a chaotic attractor (called mini) with a smaller size than the chaotic attractor of (1).

3 MSE_{1D} Algorithm

Complexity measures are important to understand and analyze systems with one dimensional data. One of the most well-known complexity measures is the multiscale sample entropy MSE_{1D}. For the time series, the computation of MSE_{1D} is defined as the following two steps:

– The first step is the coarse-graining (average) procedure, which consists in deriving a set of time series of the system dynamics on different time scales. Given a discrete time series of the form $\mathbf{x} = \{x_1, x_2, \ldots, x_i, \ldots, x_N\}$, the coarse-grained time series $\{\mathbf{y}^{(\tau)}\}$, at the scale τ, is

$$y_j^{(\tau)} = \frac{1}{\tau} \sum_{i=(j-1)\tau+1}^{i\tau} x_i, \tag{3}$$

where $1 \leq j \leq \lfloor N/\tau \rfloor$ and τ is the scale factor. If the scale factor τ is equal to one, the coarse-grained time series $\mathbf{y}^{(1)}$ corresponds to the original time series $\mathbf{x}$.

– The second step computes the sample entropy for each coarse-grained time series as the negative of the natural logarithm of the conditional probability that the sequences for m consecutive data points remain close to each other when one more point is added to each sequence $SampEn_{1D}(\mathbf{x}, m, r) = -\ln \frac{A^m(r)}{B^m(r)}$, where $A^m(r)$ is the probability that two sequences will match for $m+1$ points, whereas $B^m(r)$ is the probability that two sequences will match for m points. They are computed as

$$A^m(r) = \frac{1}{N-m} \sum_{i=1}^{N-m} A_i^m(r) \quad \text{and} \quad B^m(r) = \frac{1}{N-m} \sum_{i=1}^{N-m} B_i^m(r). \tag{4}$$

$A_i^m(r)$ is $\frac{1}{N-m-1}$ times the number of vectors $\mathbf{x}_{m+1}(j)$ within r of $\mathbf{x}_{m+1}(i)$, where j goes from 1 to $N-m$ and $j \neq i$ to exclude self-matches. $B_i^m(r)$ is $\frac{1}{N-m-1}$ times the number of vectors $\mathbf{x}_m(j)$ within r of $\mathbf{x}_m(i)$, where j goes from 1 to $N-m$ and $j \neq i$ for the same reason as above. The distance d between two vectors is defined as the maximum absolute difference of their corresponding scalar components. MSE_{1D} can be written as $MSE_{1D}(x, \tau, m, r) = -\ln \frac{A_\tau^m(r)}{B_\tau^m(r)}$, where $A_\tau^m(r)$ and $B_\tau^m(r)$ are calculated from the coarse-grained time series at the scale factor τ.

4 Equilibria and Stability

The system equilibria (2) can be found by solving the equations $\dot{x} = \dot{y} = \dot{z} = 0$. This leads to

$$\begin{cases} x - y = 0, \\ \rho x - \alpha y - \gamma xz = 0, \\ xy - \beta z = 0. \end{cases} \tag{5}$$

The first equation of the system (5) yields immediately $x = y$, so that the third one gives $z = x^2/\beta$. Therefore, the second equation leads to $z = (\rho - \alpha)/\gamma$. There are three equilibria: $X_0 = (0, 0, 0)$,

$$X_+^* = \left(+\sqrt{\frac{(\rho-\alpha)\beta}{\gamma}}, +\sqrt{\frac{(\rho-\alpha)\beta}{\gamma}}, \frac{\rho-\alpha}{\gamma} \right), \tag{6}$$

$$X_-^* = \left(-\sqrt{\frac{(\rho-\alpha)\beta}{\gamma}}, -\sqrt{\frac{(\rho-\alpha)\beta}{\gamma}}, \frac{\rho-\alpha}{\gamma} \right). \tag{7}$$

The three equilibrium points are indicated in Table 1, Table 2 and Table 3. The equilibrium points X^* depend on γ. For a variation of this parameter γ, they take place in the plane $x = y$ and on the precise curve $z = x^2/\beta$ at $(\rho - \alpha)/\gamma$.

	Classical Lorenz at. (10, 28, 1, 8/3)	Hidden attractor (4, 29, 1, 2)	Broken attractor (0.12, 0, 1, -0.6)	Chen attractor (35, -7, -28, 3)
X_0	(0, 0, 0)	(0, 0, 0)	(0, 0, 0)	(0, 0, 0)
X_+^*	(8.48, 8.48, 27)	(7.48, 7.48, 28)	(0.77, 0.77, -1)	(7.94, 7.94, 21)
X_-^*	(-8.48, -8.48, 27)	(-7.48, -7.48, 28)	(-0.77, -0.77, -1)	(-7.94, -7.94, 21)

Table 1: Three equilibrium points of the Lorenz related systems (σ, ρ, α, β, $\gamma = 1$).

	Classical Lorenz at. (10, 28, 1, 8/3)	Hidden attractor (4, 29, 1, 2)	Broken attractor (0.12, 0, 1, -0.6)	Chen attractor (35, -7, -28, 3)
X_0	(0, 0, 0)	(0, 0, 0)	(0, 0, 0)	(0, 0, 0)
X_+^*	(4.24, 4.24, 6.75)	(3.74, 3.74, 7)	(0.4, 0.4, -0.25)	(3.97, 3.97, 5.2)
X_-^*	(-4.24, -4.24, 6.75)	(-3.74, -3.74, 7)	(-0.4, -0.4, -0.25)	(-3.97, -3.97, 5.2)

Table 2: Three equilibrium points of the Lorenz related systems (σ, ρ, α, β, $\gamma = 4$).

	Classical Lorenz at. (10, 28, 1, 8/3)	Hidden attractor (4, 29, 1, 2)	Broken attractor (0.12, 0, 1, -0.6)	Chen attractor (35, -7, -28, 3)
X_0	(0, 0, 0)	(0, 0, 0)	(0, 0, 0)	(0, 0, 0)
X_+^*	(13.4, 13.4, 67.5)	(11.8, 11.8, 70)	(1.2, 1.2, -2.5)	(12.5, 12.5, 52.5)
X_-^*	(-13.4, -13.4, 67.5)	(-11.8, -11.8, 70)	(-1.2, -1.2, -2.5)	(-12.5, -12.5, 52.5)

Table 3: Three equilibrium points of the Lorenz related systems (σ, ρ, α, β, $\gamma = 0.4$).

	Classical Lorenz at. (10, 28, 1, 8/3, 1)	Hidden attractor (4, 29, 1, 2, 1)	Broken attractor (0.12, 0, 1, -0.6, 1)	Chen attractor (35, -7, -28, 3, 1)
λ_1	-8/3	-2	0.6	-3
λ_2	1.4462	8.3743	-0.12	23.836
λ_3	-12.4462	-13.3743	-1	-30.835

Table 4: Three eigenvalues of the Lorenz related systems (σ, ρ, α, β, γ) for X_0.

Linearizing (1) around X_0 provides an eigenvalue $\lambda_1 = -\beta$ along with the following characteristic equation: $\lambda^2 + (\alpha + \sigma) \cdot \lambda + \sigma \cdot (\alpha - \rho) = 0$. The two eigenvalues of this equation are indicated in Table 4, for the usual values of σ, ρ, α, β, γ. At the equilibrium point X_0, there are one positive real eigenvalue and two negative real eigenvalues. X_0 is therefore an unstable saddle point for the classical Lorenz, hidden, Chen and broken attractors. In order to study the stability of X^*, the Jacobian J_{X^*} is computed:

$$J_{X^*} = \begin{bmatrix} -\sigma & \sigma & 0 \\ \rho - \gamma z^* & -\alpha & -\gamma x^* \\ y^* & x^* & -\beta \end{bmatrix}. \tag{8}$$

Linearizing (1) around X^* yields the following characteristic equation:

$$\lambda I - J_{X^*} = \begin{bmatrix} \lambda+\sigma & -\sigma & 0 \\ -\alpha & \lambda+\alpha & \pm\sqrt{(\rho-\alpha)\beta\gamma} \\ \mp\sqrt{\frac{(\rho-\alpha)\beta}{\gamma}} & \mp\sqrt{\frac{(\rho-\alpha)\beta}{\gamma}} & \lambda+\beta \end{bmatrix} \tag{9}$$

with the characteristic polynomial $P(\lambda) = \lambda^3+(\alpha+\beta+\sigma)\lambda^2+(\rho+\sigma)\beta\lambda+2\beta\sigma(\rho-\alpha)$. This characteristic polynomial is equivalent to $P(\lambda) = \lambda^3+A\lambda^2+B\lambda+C$, where $A = \alpha+\beta+\sigma$, $B = (\rho+\sigma)\beta$, $C = 2\beta\sigma(\rho-\alpha)$. The exact values of the eigenvalues λ_1, λ_2, λ_3 can be determined by setting $\lambda = -A/3+\Lambda$. This yields $P(\Lambda) = \Lambda^3+p\Lambda+q$, where $p = -A^2/3+B$ and $q = (2A^3/27)-(AB/3)+C$. This third order polynomial in Λ can be solved using Cardan's formula, thus giving the unique real eigenvalue

$$\lambda_1 = -\frac{A}{3}+\Lambda_R = -\frac{A}{3}+\left(-\frac{q}{2}+\sqrt{\frac{q^2}{4}+\frac{p^3}{27}}\right)^{1/3}+\left(-\frac{q}{2}-\sqrt{\frac{q^2}{4}+\frac{p^3}{27}}\right)^{1/3}, \tag{10}$$

along with two complex conjugate eigenvalues

$$\lambda_{2,3} = -\frac{A}{3}-\frac{\Lambda_R}{2}\pm\frac{i}{2}\sqrt{4p+3(\Lambda_R)^2}. \tag{11}$$

The three eigenvalues of equilibrium points X^* of the classical Lorenz, Chen and broken attractors are indicated in Table 5. Since the pair of complex conjugate eigenvalues has a positive real part, the equilibrium points $X^*_\pm$ are unstable. For the equilibrium points $X^*_\pm$ of the hidden attractor, λ_1 is real and $\lambda_{2,3}$ are complex conjugates, all with negative real parts. Therefore, the equilibrium points $X^*_\pm$ are stable focus-node points.

	Classical Lorenz at. (10, 28, 1, 8/3, 1)	Hidden attractor (4, 29, 1, 2, 1)	Broken attractor (0.12, 0, 1, -0.6, 1)	Chen attractor (35, -7, -28, 3, 1)
λ_1	-13.8546	-6.8764	-0.8212	-18.4280
λ_2	$0.094+i\cdot 10.19$	$-0.062+i\cdot 8.07$	$0.1506+i\cdot 0.39$	$4.214+i\cdot 14.88$
λ_3	$0.094-i\cdot 10.19$	$-0.062-i\cdot 8.07$	$0.1506-i\cdot 0.39$	$4.214-i\cdot 14.88$

Table 5: Three eigenvalues of the Lorenz related systems (σ, ρ, α, β, γ) for $X^*_\pm$.

5 Numerical Simulations

5.1 One-parameter Lorenz related systems

Let study the Lorenz related systems, described by (2), where σ, ρ, α, β, γ are real parameters. Typically, when $\sigma = 10$, $\rho = 28$, $\alpha = 1$; $\beta = 8/3$ and $\gamma = 1$, the system is chaotic. Figure 1(a) is a graphical representation of the unique attractor on the $x-y$ plane using the *Matlab plot*(x, y) function. The magnitudes of x, y and z are $x_m = \max(x)-\min(x)$, $y_m = \max(y)-\min(y)$, $z_m = \max(z)-\min(z)$. Now, let us consider the following transformation of variables:

$$\bar{x} = \frac{x}{k}, \qquad \bar{y} = \frac{y}{k}, \qquad \bar{z} = \frac{z}{k}. \tag{12}$$

The Lorenz related system (2) can be reformulated via (12) as

$$\begin{cases} \dot{\bar{x}} = \sigma(\bar{y} - \bar{x}), \\ \dot{\bar{y}} = \rho\bar{x} - \alpha\bar{y} - (k\gamma)\bar{x}\bar{z}, \\ \dot{\bar{z}} = k\bar{x}\bar{y} - \beta\bar{z}. \end{cases} \tag{13}$$

After redefining x, y and z, the resulting system is identical to (2), but with the first term of the third equation multiplied by k. The Lorenz attractor is represented in Figure 1(b) on the $x-y$ plane with $\gamma = 1$, $k = 0.4$ ($Matlab$ $plot(\bar{x}, \bar{y})$). It can be observed that the $x-y$ representations of the systems (2) and (13) differ only by a scale factor. Furthermore, there is no scale difference with $plot(k\bar{x}, k\bar{y})$: the representation of the Lorenz attractor on $x-y$ is also identical (visual aspect and scale). Let us take again the system (2), where γ takes the value k. The unique attractor is represented graphically in Figure 1(c) on the $x-y$ plane using $plot(x, y)$. The magnitudes of x, y and z are

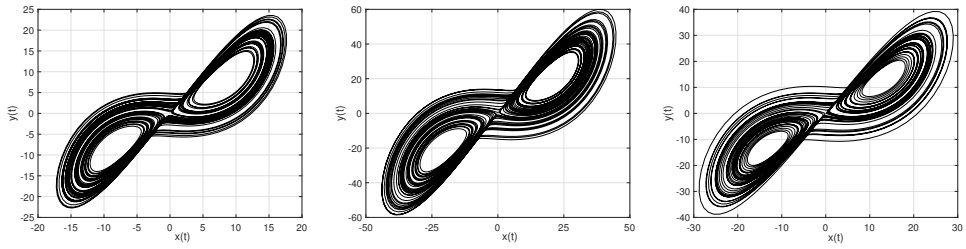

(a) (b) (c)

Figure 1: The Lorenz attractor of system (2) with $\sigma = 10$, $\rho = 28$, $\alpha = 1$, $\beta = 8/3$. (a) $\gamma = 1$, (b) $\gamma = 1$ and $k = 0.4$, (c) $\gamma = 0.4$.

$x_{m2} = \max(x) - \min(x)$, $y_{m2} = \max(y) - \min(y)$, $z_{m2} = \max(z) - \min(z)$. The $x-y$ representation of system (2) with $\gamma = 1$ and $\gamma = 0.4$ is identical, except for a scale factor. If the variables x, y and z are multiplied by x_m, y_m and z_m and divided by x_{m2}, y_{m2} and z_{m2} with $plot(x \cdot x_m/x_{m2}, y \cdot y_m/y_{m2})$, there is no more a scale difference. The two representations of the Lorenz attractor on $x-y$ and $y-z$ are also identical (visual aspect and scale).

5.2 Lorenz attractors

Figure 2(a) shows the original Lorenz attractor (grey) on the space $x-y-z$ with the initial conditions (x_0, x_0, $3 * x_0 * x_0/8$) = (1,1,3/8) and $\gamma = 1$. The result is the self-excited chaotic attractor. With a variation of γ, a mini and a maxi self-excited chaotic attractors appear in a similar manner as the well-known Lorenz attractor, but their sizes are different (Figure 2(a)). For $\gamma \in$(0,1), a maxi self-excited chaotic red attractor is generated and if $\gamma > 1$, a mini self-excited chaotic blue attractor is generated. All three attractors, mini, original and maxi self-excited chaotic attractors, have two unstable equilibria X^* on the green curve $z = x^2/\beta$. With the parameter γ, the height of the attractors is selected on this curve, as well as their size. The positive Lyapunov exponent in Table 6 for the mini and maxi self-excited chaotic attractors confirms their chaoticity. The mini and maxi chaotic attractors have different sizes and their magnitudes depend on the parameter γ. The mini and maxi chaotic attractors are not identical with the original chaotic attractor because their chaotic behaviour differs. In order to prove the similarity

and the equivalence with the original chaotic attractor, the use of multiscale entropy MSE_{1D} is proposed. Additionally, MSE_{1D} is sensitive to signal amplitude changes. A common practice to address this issue is to normalize the signal amplitude. The time series $\mathbf{x}(t)$ is rescaled along the signal amplitude axis with a factor, thus normalising the magnitude of the mini and maxi Lorenz attractors to the original Lorenz attractor. MSE_{1D} is applied to different time series of the chaotic attractors to determine their entropy over a range of temporal scales from 1 to 20. The results show (Figure 2(b)) that the MSE_{1D} increases with the variation of the scale factor for the mini, original and maxi chaotic attractors and that they have the same MSE_{1D} value. This indicates that the complexity of these attractors is at the same level.

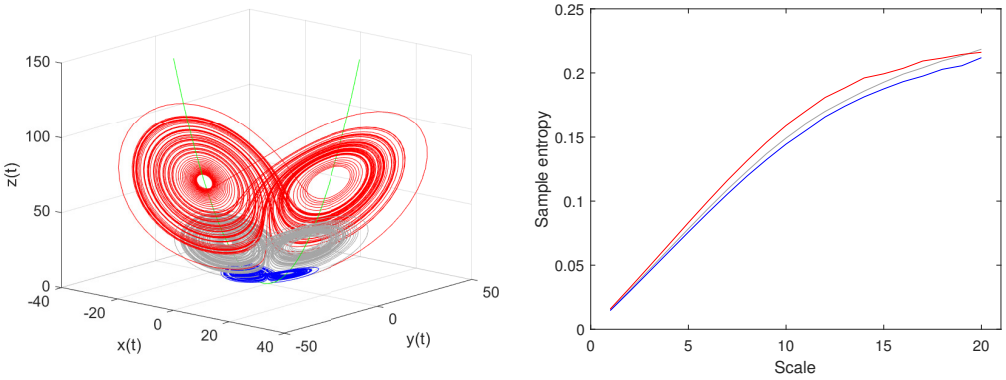

(a) Projection of phase portrait on space $x - y - z$. (b) MSE_{1D}.

Figure 2: (a) The mini ($\gamma = 4$, blue), original ($\gamma = 1$, gray) and maxi ($\gamma = 0.4$, red) Lorenz attractors with $\sigma = 10$, $\rho = 28$, $\alpha = 1$, $\beta = 8/3$; (b) MSE_{1D} of the time series of Lorenz attractors for different scales.

	Classical Lorenz at. (10, 28, 1, 8/3)	Hidden attractor (4, 29, 1, 2)	Broken attractor (0.12, 0, 1, -0.6)	Chen attractor (35, -7, -28, 3)
$\gamma = 0.4$	0.8878 0.0029 -14.5538	0.6537 0.0001 -7.6539	0.0497 0.0009 -0.57064	2.0499 0.0078 -12.0535
$\gamma = 1$	0.8904 0.0018 -14.555	0.6516 0.0005 -7.6522	0.037 -0.0025 -0.5545	2.0684 0.0015 -12.0657
$\gamma = 4$	0.8835 -0.00498 -14.5513	0.6691 0.00004 -7.6691	0.0548 0.0005 -0.668	2.0243 0.0002 -12.021

Table 6: The Lyapunov exponents of the Lorenz related systems (σ, ρ, α, β).

5.3 Hidden chaotic attractors

Figure 3(a) illustrates a hidden chaotic attractor in grey on the space $x - y - z$ using the initial conditions (x_0, y_0, z_0) = (5,5,5) and $\gamma = 1$. This attractor has the equilibria X^*

on the green curve $z = x^2/\beta$. As in the previous case, the variation of γ can generate a mini and a maxi hidden chaotic attractors. For $\gamma \in (0,1)$, a maxi hidden chaotic attractor is generated and if $\gamma > 1$, a mini hidden chaotic attractor is generated. The mini and maxi hidden attractors can be generated at any height on the z axis in the function of γ. As the parameter γ varies, an attractor appears with a periodic motion around the stable equilibrium points X^*. In this case, the rise of γ is accompanied by transformations of the attractors'size. The higher γ, the smaller the attractor (Figure 5). As we can see in Table 6, the Lyapunov exponents of the mini and maxi hidden chaotic attractors are positive. MSE_{1D} is now applied to different time series of the hidden chaotic attractor

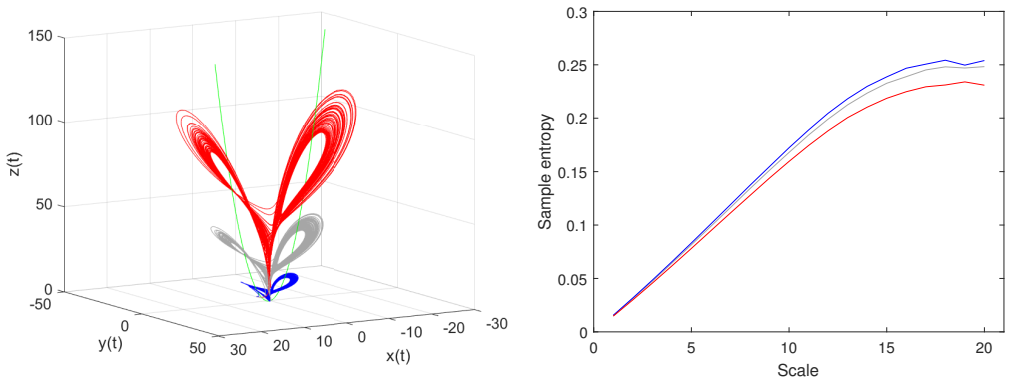

(a) Projection of phase portrait on space $x - y - z$. (b) MSE_{1D}.

Figure 3: (a) The mini ($\gamma = 4$, blue), original ($\gamma = 1$, gray) and maxi ($\gamma = 0.4$, red) hidden chaotic attractors with $\sigma = 4$, $\rho = 29$, $\alpha = 1$, $\beta = 2$, with (x_0, y_0, z_0) = (5,5,5); (b) MSE_{1D} of the time series of hidden chaotic attractors for different scales τ.

and of the one point attractor to qualify entropy over a range of temporal scales for $\tau =$ 1 to 20. The mini, original and maxi chaotic attractors have the same MSE_{1D} values for the small time scales (Figure 3(b)); very small differences appear for the large time scales. MSE_{1D} values of the mini, original and maxi one point attractors are identical at the begining of the scale, and with small differences in the end of the scale, as in Figure 3(b). The complexity of the chaotic sequences tends to be uniform, independently of γ.

5.4 Broken butterfly attractors

Figure 4(a) illustrates the broken butterfly attractors in grey on the space $x-y$, where two strange attractors coexist ((x_0, y_0, z_0) = (-0.8,3,0), (x_0, y_0, z_0) = (0.8,-3,0) and $\gamma = 1$). Starting from the same initial conditions, for $\gamma = 0.4$, two strange maxi broken butterfly chaotic attractors are generated. If $\gamma = 4$, two other strange mini broken butterfly chaotic attractors are also generated. The positive Lyapunov exponents of the mini and maxi self-excited chaotic butterfly attractors confirm their chaoticity. The magnitudes of the broken butterfly chaotic attractors of the mini ($\gamma = 4$), original ($\gamma = 1$) and maxi ($\gamma =$ 0.4) are different: they vary from 1 for the mini broken butterfly attractor to 4 for the maxi broken butterfly attractor on the x-axis. The irregularity values MSE_{1D} of the three broken butterfly attractors are identical for the small time scales, while very small differences appear for the large time scales, as shown in Figure 4(b).

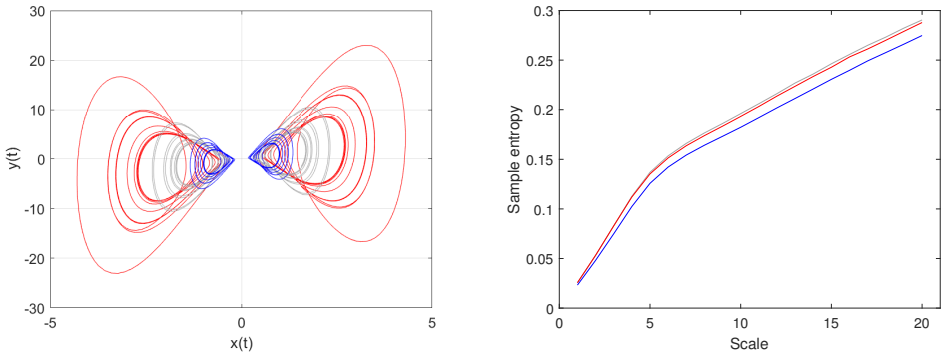

(a) Coexisting strange attractors on the $x-y$ plane for $\gamma = 0.4$, 1, 4 and two symmetric initial conditions (∓ 0.8, ± 3, 0).

(b) MSE_{1D} of the time series of broken attractors for different scales τ.

Figure 4: Broken attractors with $\sigma = 0.12$, $\rho = 0$, $\alpha = 1$, β = -0.6.

5.5 Chen chaotic attractors

Figure 5(b) illustrates the Chen attractor in grey on tri-dimensional space with $\gamma = 1$. For $\gamma = 0.4$, a maxi Chen red attractor is generated (Figure 5(a)) and if $\gamma = 4$, a mini Chen blue attractor is generated (Figure 5(c)). A graphical comparison is given in Figures 5(a), (b), (c), where the maxi, original and mini Chen attractors are represented on the $y-z$ plane. The mini and maxi Chen attractors are visually similar to the original Chen attractor (Figure 5(b)), but not identical. The chaotic behaviour of all attractors is proved by the positive Lyapunov exponents in Table 6.

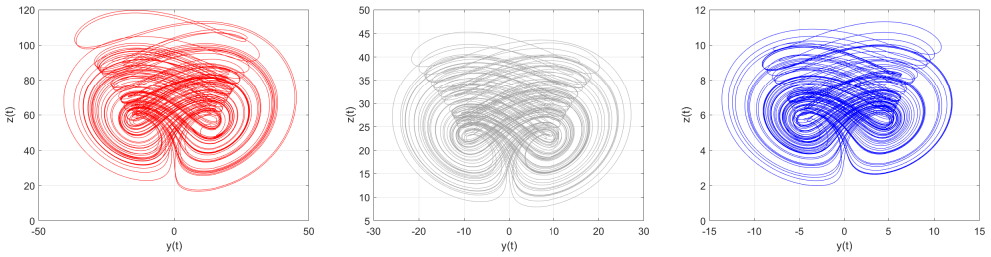

(a) Maxi attractor $\gamma = 0.4$.

(b) Original attractor $\gamma = 1$.

(c) Mini attractor $\gamma = 4$.

Figure 5: The Chen chaotic attractor for $\sigma = 4$, $\rho = 29$, $\alpha = 1$, $\beta = 2$ with $(x_0, y_0, z_0) = (0.1, 0, 0)$.

As shown in Figures 5(c), (b), (a), the magnitudes of the Chen attractors of the mini ($\gamma = 4$), original ($\gamma = 1$) and maxi ($\gamma = 0.4$) attractors are different. The magnitude of the original attractor is 40 (Figure 6 (a)), but for the mini and maxi attractors, the magnitudes are 10 and 100, respectively. The multiscale entropy MSE_{1D} is employed to quantify the complexity of the time series of mini and maxi Chen attractors over the same scales for $\tau = 1$ to 20 with the original Chen attractor: the mini, original and maxi chaotic attractors have the same MSE_{1D} (Figure 6(b)).

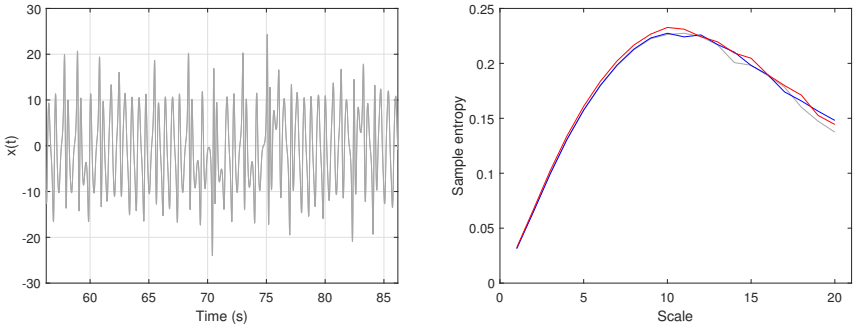

(a) Time series of $x(t)$ for $\gamma = 1$.

(b) MSE_{1D} of the time series of the Chen attractors for different scales.

Figure 6: The Chen attractors with the parameters $\sigma = 35$, $\rho =$ -7, $\alpha =$ -28, $\beta = 3$.

6 Bifurcation Diagrams, Lyapunov Exponents and Multiscale Entropy MSE_{1D} Analysis of Chen Attractors

In the previous section, three chaotic Chen attractors were presented for a unique value of the parameter $\beta = 3$. In this section, we are interested in the dynamic behaviour of Chen system for a large variation of this parameter β changing gradually from the lower to the upper values of $\beta = [1, 7]$. This system can generate chaotic dynamic behaviours in a wide region of β. Figures 7, 8 and 9 show the bifurcation diagrams and the largest Lyapunov exponent of the Chen system (with the parameters $\sigma = 35$, $\rho =$ -7, $\alpha =$ -28) for $\gamma = 0.4$, 1 and 4. In order to prove the similarity and the equivalence of different size Chen attractors ($\gamma > 1$ or $\gamma < 1$) with the original Chen attractor ($\gamma = 1$), the MSE_{1D} is applied to different time series of the chaotic attractors to measure their degree of irregularity and disorder. It evaluates the probability of finding similar patterns.

Using the Poincaré map method, the bifurcation values are computed from the time series $\mathbf{x}(t)$, against the bifurcation parameter β. The three bifurcation diagrams have an almost identical structure apart from a scale dimensioning on the ordered axis. The maxi, original and mini Chen chaotic attractors depend on the amplitude of the variables $x(t)$, $y(t)$ and $z(t)$, where $x(t)$ is involved in the bifurcation diagrams. The attractors have a higher size at a greater amplitude of bifurcation diagrams. The largest Lyapunov exponent is calculated to analyze the dynamic Chen system for $\mathbf{x}(t)$. It can be observed that the largest Lyapunov exponent values (Figures 7(b), 8(b) and 9(b)) properly reflect the behaviour of the Chen system presented in the bifurcation diagrams (Figures 7(a), 8(a) and 9(a)). Furthermore, these figures show the same bifurcation scenario and the same Lyapunov exponents for the same values of β and independently of γ.

Additionally, MSE_{1D} is sensitive to the signal amplitude changes. A common practice to address this issue is to normalize the signal amplitude. The time series $\mathbf{x}(t)$ is rescaled along the signal amplitude axis with a factor, thus normalising the magnitude of the mini and maxi Chen attractors to the original Chen attractor. The MSE_{1D} is applied to determine their entropy over a scale τ from 1 to 20. The complexity of the Chen system is analyzed by varying the system parameter β from 1 to 7 with a 0.01 step. The results show (Fig. 10) that the mini, original and maxi chaotic attractors have almost the same MSE_{1D} values for all time scales. For the region $\beta \in [5, 7]$, the Chen

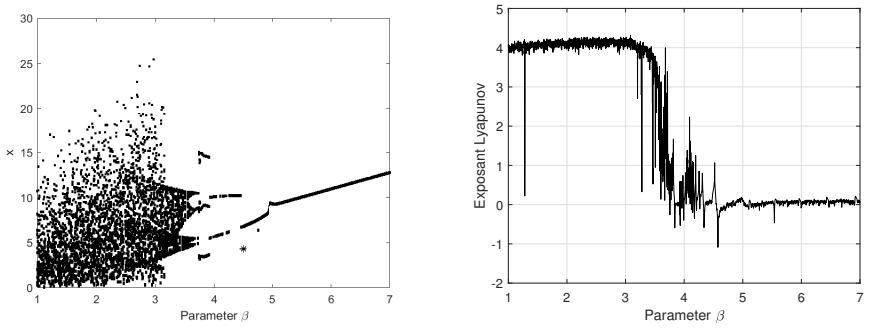

(a) (b)

Figure 7: (a) The bifurcation diagram and (b) the largest Lyapunov exponent plotted against the bifurcation parameter β with $\sigma = 35$, $\alpha = 28$ and $\gamma = 0.4$.

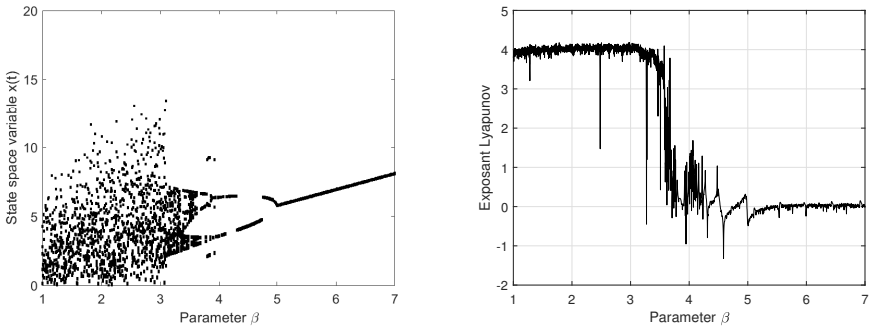

(a) (b)

Figure 8: (a) The bifurcation diagram and (b) the largest Lyapunov exponent plotted against the bifurcation parameter β with $\sigma = 35$, $\alpha = 28$ and $\gamma = 1$.

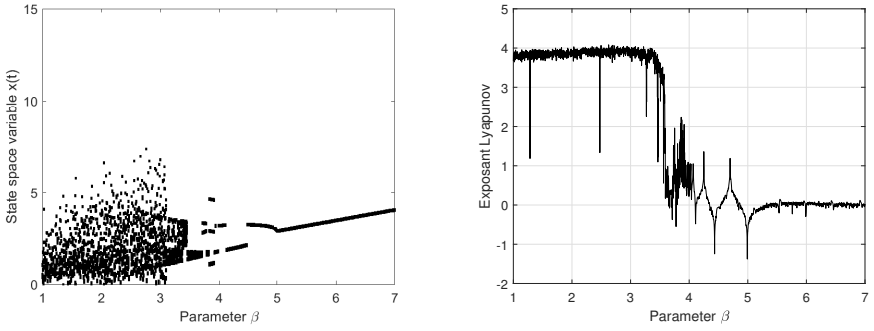

(a) (b)

Figure 9: (a) The bifurcation diagram and (b) the largest Lyapunov exponent plotted against the bifurcation parameter β with $\sigma = 35$, $\alpha = 28$ and $\gamma = 4$.

system behaves as a limit cycle attractor, with a simplest behaviour of x. However, when the largest Lyapunov exponent of the system is approximately equal to zero, it corresponds to the oscillations before the first bifurcation point. More specifically, the MSE_{1D} values of the mini, original and maxi periodic attractors are zero (Fig. 10), which indicates a lower complexity. However, the MSE_{1D} surface begins to contain nonzero values after the first bifurcation point. In the range, after the first bifurcation point and before the second bifurcation, the system has an irregular behaviour. After this second bifurcation, the complexity of the oscillations continues to rise. It should be pointed out that for $\beta \in [3.69, 3.8]$, the Chen system has an abundant dynamic behaviour. For this tight interval of β, the original attractor sometimes has the same behaviour as the mini attractor or the maxi attractor or, occasionally, both. For $\beta = 3.73$, Fig. 11 shows the phase portraits of three attractors for $\gamma = 0.4$, 1 and 4. There is a similarity between the two first orbits, but not with the last one. An interesting observation is that the doubling-period bifurcations depend on the parameter γ. Decreasing more $\beta = 3.72$, the periodic orbit of Fig. 11 (a), (b) evolves into the behaviour shown in Fig. 12 (a), (b). Indeed, the Chen system represents the transition from one behaviour to another when the parameter β is slowly varied. Furthermore, the generated mini and maxi attractors are similar to the original attractor, but they have different sizes. The qualitative properties are preserved independently of γ. As shown in Figs. 7, 8 and 9, the Chen system can evolve into the chaotic attractors when $\beta \in [1, 3.69]$. The positive Lyapunov exponents for the mini, original and maxi Chen attractors confirm their chaoticity. Compared with the Lyapunov exponents and bifurcation diagrams, the MSE_{1D} complexities are consistent, which means that complexity can also reflect the chaotic characteristics of the Chen system. MSE_{1D} has small values for the periodic behaviour and increases when the attractor moves from a period to chaos, as in Figure 10. According to the above analysis, the complexity of different attractors has the same level independently of γ and their sizes (the same maximum Lyapunov exponent values, the same MSE_{1D} values). The complexity of the mini ($\gamma = 4$) and maxi ($\gamma = 0.4$) attractors is similar to that of the original attractors ($\gamma = 1$). Moreover, Fig. 13 shows that the complexity decreases with β in the sense of the MSE_{1D} values. To improve the understanding of the Chen attractor behaviour for small values of $\beta < 3$ and for a scale factor $\tau = 1$ (Figure 13), the relative error of MSE_{1D} is calculated. It is very useful to compare attractors of different size to the reference one (the original attractor). This alternative is also used to measure the complexity of attractors that visually look like the original attractor. The accuracy of attractors of different size determines how far this one is from the original attractor. It is often helpful to present numbers as percentages as this gives a sense of proportion. The relative error of MSE_{1D} of the mini and maxi Chen attrators reported to the original Chen attractor is based on the absolute error of the MSE_{1D}. Figure 14 (a) shows the absolute error of the MSE_{1D} of the Chen system with $\gamma = 0.4$ compared to the MSE_{1D} of the original Chen system with $\gamma = 1$. A similar figure (Fig. 14(b)) is obtained from the difference between the MSE_{1D} of the Chen system with $\gamma = 4$ and the MSE_{1D} of the original Chen system with $\gamma = 1$. Figure 14 shows a very small absolute error of 0.005 for the chaotic behaviour and 0 for the periodic behaviour. The mean value of the absolute error of MSE_{1D} is zero for the periodic attractor ($\beta > 4$) and increases to 0.0027, respectively, 0.0023, when the system is in the route to chaos (β <3). Figure 15 (a), (b) shows the relative error of MSE_{1D} for the Chen attractors with $\gamma = 0.4$, $\gamma = 4$ compared to the MSE_{1D} of the Chen attractor with $\gamma = 1$. The MSE_{1D} mean relative error is zero for the periodic attractor ($\beta > 4$) and increases to 6.65 %,

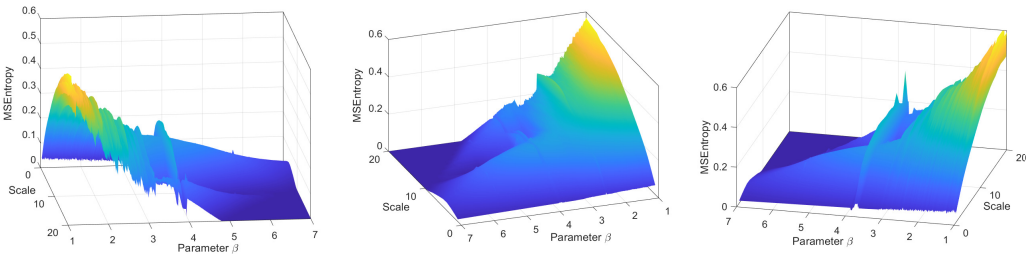

(a) $\gamma = 0.4$ (b) $\gamma = 1$ (c) $\gamma = 4$

Figure 10: MSE_{1D} of $x(t)$ for different scales and for $\sigma = 35$, $\alpha = 28$, $\beta = 3$.

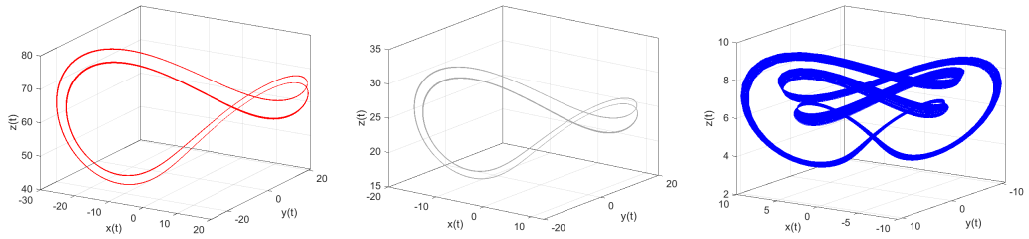

(a) $\gamma = 0.4$ (b) $\gamma = 1$ (c) $\gamma = 4$

Figure 11: The phase portraits of the chaotic attractors for $\sigma = 35$, $\alpha = 28$, $\beta = 3.73$.

respectively, 5.73 %, when the system is in the route to chaos (β <3), as in Figure 15 (a), respectively, (b). In fact, the rise of complexity is significant to MSE_{1D} for $\tau > 1$ and not for $\tau = 1$. Quantitatively, the relative error of MSE_{1D} for the Chen attractors with $\gamma = 0.4$ and $\gamma = 4$ compared to the MSE_{1D} for the original Chen attractor with $\gamma = 1$ is very small, almost insignificant. We can finally conclude that the MSE_{1D} values depict that the complexity of chaotic systems is independent of the size of attractors and matches well with the largest Lyapunov exponent and the bifurcation diagram.

7 Conclusions

In this paper, the dynamic behaviour of the Lorenz system is examined in a previously unexplored region of the parameter γ. The variation of this parameter reveals that the chaotic Lorenz related systems can generate strange attractors of different sizes. The use of bifurcation diagrams and the Lyapunov exponents is proposed to study the global dynamic behaviour of the Chen attractor. Through the theoretical analysis and mathematical simulations, the multiscale entropy MSE_{1D} of different time series under the γ variation parameter is calculated, qualifying the chaotic attractors' irregularity. The complexity of the chaotic sequences tends to be uniform, independent of the γ variation. It is noticeable that all their quantitative properties are preserved for any value of γ. Finally, throught the MSE_{1D}, the complexity of chaotic systems is independent of the size of attractors and matches well with the largest Lyapunov exponents and bifurcation diagrams.

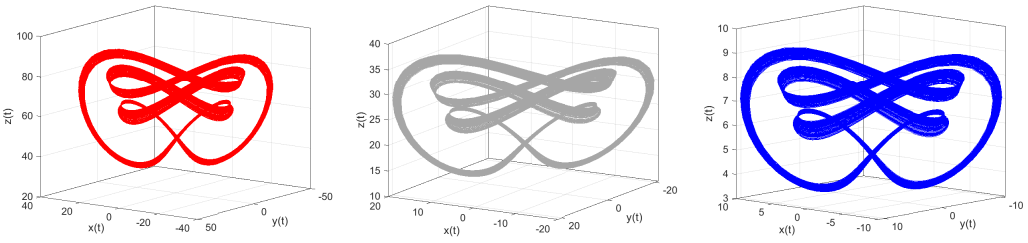

(a) $\gamma = 0.4$ (b) $\gamma = 1$ (c) $\gamma = 4$

Figure 12: The phase portraits of the chaotic attractors for $\sigma = 35$, $\alpha = 28$, $\beta = 3.72$.

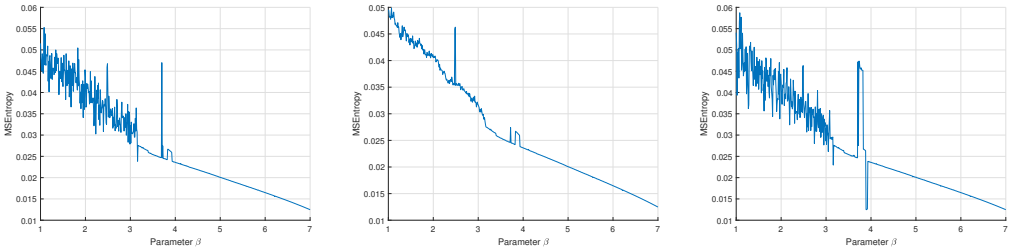

(a) $\gamma = 0.4$ (b) $\gamma = 1$ (c) $\gamma = 4$

Figure 13: MSE_{1D} of $x(t)$ of the Chen attractor for $\tau = 1$, $\sigma = 35$, $\alpha = 28$.

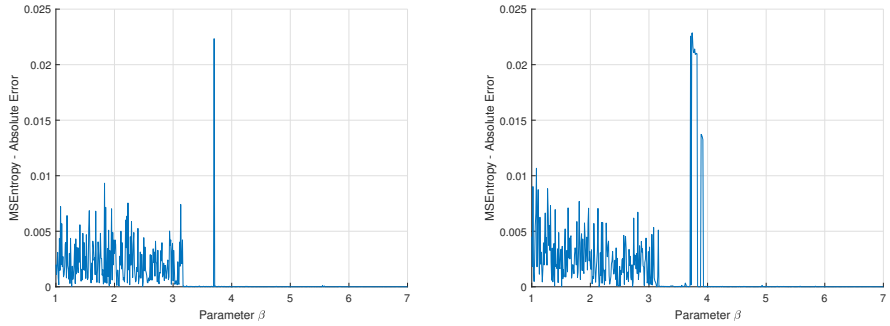

(a) $\gamma = 0.4$ (b) $\gamma = 4$

Figure 14: (a) The absolute error of MSE_{1D} for the Chen attractor with $\gamma = 0.4$ and $\gamma = 4$ compared to the MSE_{1D} with $\gamma = 1$.

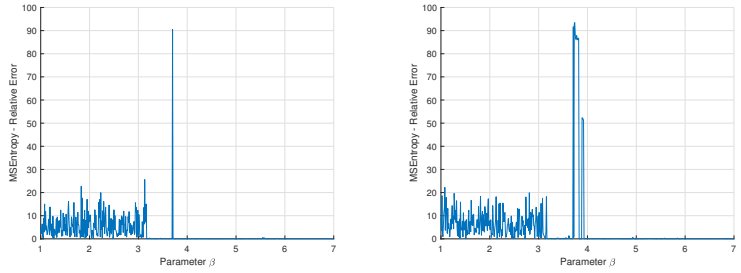

(a) $\gamma = 0.4$ (b) $\gamma = 4$

Figure 15: The relative error of MSE_{1D} for the Chen attractor with $\gamma = 0.4$ and $\gamma = 4$ compared to the MSE_{1D} with $\gamma = 1$.

References

[1] J. Lu, G. Chen and S. Zhang. A hidden chaotic attractor in the classical Lorenz system. *International Journal of Bifurcation and Chaos* **12** (2002) 1001–1015.

[2] J. Lu, G. Chen, S. Zhang and S. Celikovsky. Bridge the gap batween the Lorenz system and the Chen system. *International Journal of Bifurcation and Chaos* **12** (2002) 2917–2926.

[3] R. Barboza. On Lorenz to Chen system. *International Journal of Bifurcation and Chaos* **28** (2018) 1850018.

[4] C. Li and J C. Sprott. Multistability in the Lorenz system: A broken butterfly. *International Journal Bifurcation and Chaos* **24** (2014) 1450131.

[5] S. Jafari and J. Sprott. Simple chaotic flows with a line equilibrium. *Chaos, Soliton and Fractals* **57** (2013) 79–84.

[6] Z. Wei and G. Chen. Dynamical behaviors of a chaotic system with no equilibria. *Phys. Lett. A* **376** (2011) 102–108.

[7] M. Molaie, S. Jafari, J. C. Sprott and S. Golpayegani. Simple chaotic flows with one stable equilibrium. *International Journal Bifurcation and Chaos* **23** (2013) 1350188–1–7.

[8] J. C. Sprott, S. Jafari, V. T. Pham and Z. S. Hosseini. A chaotic system with a single unstable node. *International Journal of Computer Mathematics* **379** (2015) 2030–2036.

[9] C. Morel and R. Vlad. A new technique to generate independent chaotic attractors in the state space of nonlinear dynamics systems. *Nonlinear Dynamics* **59** (2009) 45–60.

[10] G. A. Leonov, N. V. Kuznetsov and T. N. Mokaev. Hidden attractor and homoclinic orbit in Lorenz-like system describing convective fluid motion in rotating cavity. *Commun. Nonlinear Sci. Numerical Simulation* **28** (2015) 166–174.

[11] A. Ouannas. A new synchronization scheme for general 3D quadratic chaotic systems in discrete-time. *Nonlinear Dynamics and Systems Theory* **15** (2015) 163–170.

[12] S. Kaouache, N. E. Hamri, A. S. Hacinliyan, E. Kandiran, B. Deruni and A. C. Keles. Increased Order Generalized Combination Synchronization of Non-Identical Dimensional Fractional-Order Systems by Introducing Different Observable Variable Functions. *Nonlinear Dynamics and Systems Theory* **20** (2020) 107–115.

[13] C. Liu, L. Ding and Q. Ding. Research about the characteristics of chaotic systems based on multi-scale entropy. *Entropy* **21** (2019) 663.

[14] C. Morel and A. Humeau. Multi-scale permutation entropy for two-dimensional patterns. *Pattern Recognition Letters* **150** (2021) 139–146.